

Quantitative electronic stopping power from localized basis set

Ivan Maliyov, Jean-Paul Crocombette, and Fabien Bruneval ^{*}

DEN, Service de Recherches de Métallurgie Physique, CEA, Université Paris-Saclay, F-91191 Gif-sur-Yvette, France



(Received 22 November 2019; published 21 January 2020)

The electronic stopping power of a swift ion in matter can be obtained from *ab initio* calculations within time-dependent density functional theory. Most implementations rely today on a plane-wave plus pseudopotential approach, but at the expense of very cumbersome calculations. We show here that localized orbitals, especially with Gaussian-type orbitals, are a valuable alternative. These calculations can yield electronic stopping powers in quantitative agreement with the plane-wave results while maintaining a computational burden that is relatively low. These positive results are possible only when using Gaussian basis sets that were specially designed for the stopping power calculations. With this tool, we investigate the discrepancy between *ab initio* calculations and experiment at large velocity, the effect of the exchange-correlation functional, and the role of core excitations in the total stopping power. We rule out the widespread centroid path approximation as soon as the core electrons are involved in the process.

DOI: [10.1103/PhysRevB.101.035136](https://doi.org/10.1103/PhysRevB.101.035136)

I. INTRODUCTION

The interaction between a fast irradiating ion and a target material is essential in many technological and scientific fields, such as nuclear material science [1], medicine [2], focused beam techniques [3], semiconductor physics [4], etc. The slowing down of an ionic projectile in a host material is quantified by the stopping power S , defined as the energy transfer from the projectile to the target per penetration distance. The most significant ionic energy loss channels in the irradiation process are the electronic excitations [5], which give rise to the so-called electronic stopping power S_e .

In the previous century, most electronic stopping power evaluations used model electronic systems to limit the numerical burden. Homogeneous electron gas [6–10] and spherical atoms [11–13] were important examples of such model systems. However, nowadays the real-time time-dependent density-functional theory (RT-TDDFT) [14] provides probably the best compromise between the accuracy and the size of atomic systems one can deal with for the electronic stopping power *ab initio* simulations [15]. The stopping power calculation within the RT-TDDFT approach is implemented in several codes that follow different numerical approaches: plane-wave basis set (QBOX/QB@LL [16,17]), real-space grid (OCTOPUS [18]), and localized basis (SIESTA [19,20], CP2K [21], MOLGW [22]). Each implementation has its advantages and drawbacks. The plane-wave approach is the most straightforward choice; however, the stopping power calculations are reported to necessitate massive supercomputer facilities [23,24], especially when core electrons enter into play [17]. At the opposite end of the spectrum, the localized atomic bases are, in principle, much more affordable and are able to treat valence and core electrons at once [25]. However,

doubts about the ability to reach an absolute convergence exist [13,26].

In this paper, we aim at demonstrating that a target convergence level can be achieved for the electronic stopping power using atomic-centered Gaussian orbitals. Gaussian-type orbitals are the workhorse of quantum chemistry [27], and numerous codes use them in practice. These basis functions simply read as the product between a solid harmonics angular part and a radial part:

$$\phi(\mathbf{r}) = \mathcal{Y}_l^m(\hat{\mathbf{r}}) r^l \sum_b c_b e^{-\alpha_b r^2}, \quad (1)$$

where l is the angular momentum, m is its projection, $\mathcal{Y}_l^m(\hat{\mathbf{r}})$ are real spherical harmonics, and c_b are the contraction coefficients of the primitives that are fixed for a given basis set. The spatial extension of a basis function is governed by the smallest exponent α_b : the smaller the exponent is, the more diffuse the function is.

Our RT-TDDFT is built on MOLGW [22]. In this code, the basis functions are centered around the target atoms, whereas the ionic projectile is modeled as a bare Coulomb potential. In doing so, most quantities (basis functions, Coulomb integrals, overlap matrices, etc.) do not change along with a simulation and can be precalculated and stored in the beginning. We also exploit the possibility to employ different basis sets on different atoms to describe accurately only the region where the electronic excitations take place. All these features are unique to localized orbitals and play a major role in the numerical efficiency of the approach.

This paper is organized as follows: Sec. II is a short recap of the methodology to obtain random electronic stopping power from *ab initio* calculations. Section III is devoted to Gaussian basis convergence with regular basis sets and with custom basis sets especially tailored for the electronic stopping power. With these unique basis sets, we will address a few open questions for the community in Sec. IV: How does RT-TDDFT compare to experiment? Is the approximate

^{*}fabien.bruneval@cea.fr

exchange-correlation contribution responsible for the discrepancy with respect to experiment at large velocity? How significant are the core excitations as a function of the ion velocity? Is the centroid path approximation valid? Most of our calculations will be exemplified for proton and α -particle irradiations on crystalline aluminum since this system is very well studied in the experiment and with other TDDFT schemes, both within the linear-response approximation [28] and beyond [17].

II. RANDOM ELECTRONIC STOPPING POWER IN TDDFT

Electronic stopping power calculations were described at length in several previous articles [15,20,25,29]. However, for clarity, we would like to repeat here the most salient features of this type of calculation.

We follow the most widely used approach in which the electronic stopping power is simulated by an ion moving linearly at constant velocity v through a lattice of fixed atoms [20]. With this simple approach, we neglect the so-called nuclear electronic stopping power. This approximation is very accurate for the range of ion velocities considered here ($v \geq 0.1$ a.u.). As we impose a constant velocity, we apply work to the system, and therefore, the total energy of the system increases. The applied work precisely compensates the kinetic energy loss of the ion. As a consequence, the increase of total energy ΔE per unit length Δz is exactly the electronic stopping power:

$$S_e(v) = \frac{\Delta E}{\Delta z}. \quad (2)$$

As the ions impinging the sample come as a parallel beam, experiments measure the impact-parameter-averaged stopping power, which is named *random* electronic stopping power (RESP). Some authors use long tilted trajectories in crystalline material to mimic the impact parameter averaging [17,30]. We demonstrated recently an alternate route [25]: We employ a series of independent trajectories in a large enough cluster to simulate the bulk crystal. The impact parameters are sampled in a central unit tile that can pave the entire surface. The design of the unit tile and the details of the averaging method are recalled in the Appendix. Here we use 13 different impact parameters for the aluminum target to sample the RESP.

In practice, we use a cylindrical cluster of 54 aluminum atoms for the final RESP calculations. The cluster axis is oriented along the ion path. Here we chose the [001] orientation. We showed in Ref. [31] that the orientation does not matter for the RESP. The fast convergence with respect to the cluster size was appraised in our previous study [25].

The use of localized orbitals allows us to employ different basis sets on different atoms. We showed in Ref. [25] that only the 14 central atoms require a large basis set. Then, a smaller basis set is assigned to eight atoms that are located at intermediate distance from the projectile track [namely, Dunning correlation-consistent polarized valence quadruple zeta (cc-pVQZ)]. The outer atoms are simply described with the smallest basis of the Dunning family [correlation-consistent polarized valence double zeta (cc-pVDZ)]. We had called this procedure the mixed basis approach. In the rest of the

paper, we change only the central region basis functions, and therefore, we name the results after the basis set used in the central region.

For the basis set optimization described in the next section (and only in that section) we use a smaller cluster of 22 atoms to save computational resources. Only the basis functions for the 14-atom central part will be optimized.

III. OPTIMIZED LOCALIZED BASIS

In this section, we first review the stopping power results obtained with standard quantum chemistry bases and show that they are insufficient. We then propose an automated construction of basis sets specifically optimized for the stopping power calculations. Proton irradiation in aluminum will serve as an example in this section.

A. Standard basis

We exemplify the Gaussian basis convergence problem by using the common Dunning basis sets [32,33]. These bases are constructed in a way to provide smooth and monotonic convergence for the correlation energy [34]. The Dunning basis sets are characterized by the so-called cardinal number X . Switching from an $X - 1$ to an X basis, the maximal orbital momentum of the basis set is incremented by one unit, and one extra shell is added for all the included angular momenta. For aluminum, the value of X coincides with the largest orbital momentum included in the basis set. The standard Dunning sets cc-pVXZ can be augmented by the inclusion of diffuse basis functions (aug-cc-pVXZ) or tight-core functions (cc-pCVXZ) or both (aug-cc-pCVXZ).

We have observed that for the electronic stopping power calculations, both diffuse, aug-..., and tight-core, ...-pCVXZ, basis functions are indeed necessary to obtain accurate values of S_e : Diffuse functions are important for small projectile velocities ($v \leq 1.0$ a.u. in the Al case), while the core functions have a significant contribution at high velocities ($v > 2.0$ a.u. in the Al case).

Figure 1(a) presents the RESP convergence of a proton projectile in an aluminum cluster for the most complete Dunning basis set family aug-cc-pCVXZ. Here we use a cluster size large enough to approach the bulk limit, as explained in Ref. [25]. Remember that we use a mixed-basis technique [25], where we assign the more precise basis sets (aug-cc-pCVXZ) to the target atoms that are close to the projectile track while keeping all the other atoms described within the fixed smaller basis sets (as described in the previous section).

Figure 1(a) shows the high sensitivity of the electronic stopping power to the basis set: The difference between the smallest presented basis (aug-cc-pCVDZ) and the largest one (aug-cc-pCV6Z) varies from 40% to 70%. It is also seen that the difference between the two most complete bases (aug-cc-pCV6Z and aug-cc-pCV5Z) is still far from being negligible. Therefore, the aug-cc-pCV6Z basis set cannot be considered converged.

The Dunning basis sets are consistently built to be able to extrapolate the results to the complete basis set limit [33,34]. We propose to follow the same approach for our observable, the RESP.

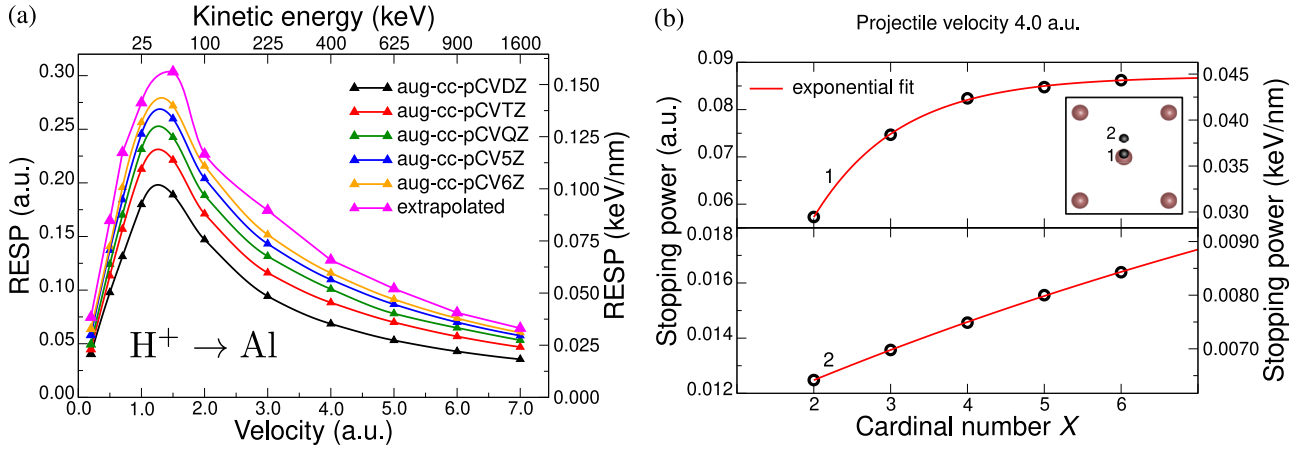


FIG. 1. (a) Dunning basis set convergence of the random electronic stopping power of a proton in aluminum. (b) Electronic stopping power convergence in aluminum for two proton impact parameters: $p_1 = 0.1 \text{ \AA}$ (top panel) and $p_2 = 1.3 \text{ \AA}$ (bottom panel); the projectile velocity is $v = 4.0 \text{ a.u.}$ Inset: the front view of the [001] aluminum cluster. Aluminum atoms are depicted as pink spheres, and the two proton impact parameters are shown as black spheres.

Trying many analytic forms, we have observed that the following expression best fits our convergence rate for the stopping power:

$$\langle S_e(X) \rangle = S_\infty - S_1 \exp(-aX), \quad (3)$$

where $\langle S_e(X) \rangle$ is the RESP at a given projectile velocity, X is the basis cardinal number, and S_∞, S_1, a are three fitting coefficients that are, of course, velocity dependent. S_∞ is then the complete-basis-set-limit RESP. It is represented in pink in Fig. 1(a). Note that a similar function was used by Yao and coworkers [35] for the extrapolation of the stopping power as a function of the plane-wave cutoff in order to describe the K -shell excitations of water under the proton irradiation.

The line shape of the extrapolated curve differs noticeably from the calculation with the largest basis set (aug-cc-pCV6Z). Indeed, different impact parameters have different convergence rates. Figure 1(b) shows the convergence for two projectile impact parameters p at the same velocity $v = 4.0 \text{ a.u.}$: one close to a target nucleus ($p = 0.1 \text{ \AA}$) and one distant from it ($p = 1.3 \text{ \AA}$). While the stopping power for a projectile trajectory close to the nucleus has a convergent behavior, the curve corresponding to a larger impact parameter is almost linear. The RESP is the average over the projectile impact parameters (details are given in the Appendix). The extrapolation uncertainties at large impact parameters permeate all the way to the final averaged quantity.

The electronic stopping power is then very sensitive to the Gaussian basis set. To obtain the converged result using standard basis sets, one needs to perform a computationally expensive procedure: calculate the stopping power for the whole range of several large basis sets and then extrapolate. The slow convergence of RESP with respect to the cardinal number X demonstrates that the standard basis sets are not well adapted for the electronic stopping power calculations. This is not surprising: Electronic stopping is a process that involves very energetic excitations of presumably almost all electrons of the target.

Taking these considerations into account, we have decided to develop an optimization procedure to design Gaussian basis sets specifically for the electronic stopping power.

B. Algorithm for the stopping-power-optimized basis set generation

Optimizing basis sets for a specific observable is regularly carried out in quantum chemistry: See Ref. [36] for ground-state electron momentum density and Ref. [37] for high-harmonic generation spectroscopy. This section aims at defining a generation procedure for the RESP.

We observe from Fig. 1 that the RESP increases when the basis set completeness improves. In almost all of our calculations, we have experienced such behavior. Independent plane-wave calculations also experience this phenomenon [35]. Even though we were not able to prove it mathematically for TDDFT, this increase is very intuitive: When improving the completeness of the basis for the unoccupied states, one opens up new electronic excitation processes and therefore new loss channels for the projectile.

Our basis optimization procedure consists then of *maximizing* the random stopping power for a system as close as possible to the final system of interest at a given velocity v_0 .

The generic Gaussian-type orbital form is shown in Eq. (1). For simplicity, we will stick to atom-centered functions and to uncontracted Gaussians. Hereafter, the coefficients c_b are always unity, and we will omit the subscript b from α_b . The optimization plays with two parameters: the orbital momentum l and the Gaussian exponent α . A Gaussian exponent gives rise to a so-called shell of orbitals: for instance, three p orbitals sharing the same Gaussian radial part.

Let us describe the algorithm:

(0) We start with an initial guess for the basis labeled opt0. This basis must contain at least the minimal set of functions needed to describe the occupied electronic states. For the proton in aluminum, to obtain opt0, we take all the s and p shells contained in the cc-pCVQZ basis.

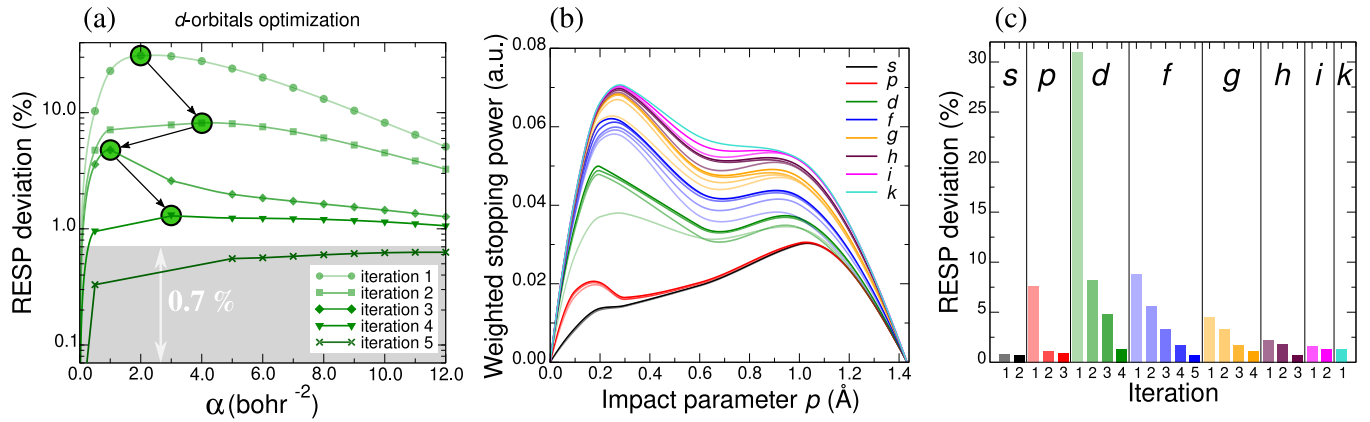


FIG. 2. Basis set optimization procedure exemplified for a swift proton ($v_0 = 4.0$ a.u.) in aluminum. (a) Change in random electronic stopping power for a basis set with the addition of a shell with exponent α or without it. The exponent that corresponds to the maximal change is selected to be part of the optimized basis set. The gray area visualizes the deviation lower than the target accuracy (chosen to be 0.7%). (b) The electronic stopping power multiplied by the weight function that corresponds to the geometry of the target (see the Appendix for details) as a function of the impact parameter. The colors of the curves correspond to different orbital momenta. Curves corresponding to incomplete convergence for the same l have dimmer shades. (c) Stopping power deviations as a function of the optimization step number for each angular momentum l . The color scheme of sectors is consistent across (a), (b), and (c).

We perform the optimization, one orbital momentum after the other, from $l = 0$ to $l = l_{\max}$. Here we use $l_{\max} = 7$. During steps 1 to 3 the value of l is fixed.

(1) We define a candidate list of Gaussian exponents $\{\alpha^{(i)}\}$ that encompasses a wide range (typically, from $\alpha = 10^{-3}$ bohr $^{-2}$ to $\alpha = 20$ bohr $^{-2}$) but that omits the α 's already present in the current basis for angular momentum l .

(2) For each candidate $\alpha^{(i)}$, we add a shell with this Gaussian exponent to the basis set with angular momentum l and calculate the RESP with the current basis augmented with the candidate shell, $\langle S_e(\alpha^{(i)}) \rangle$ (the projectile velocity being equal to v_0). Note that this step consists of several trajectories with different impact parameters for each candidate.

(3) Among all the values in $\{\langle S_e(\alpha^{(i)}) \rangle\}$, we select the $\alpha^{(i)}$, called α^{max} , that maximizes the RESP. If the relative deviation of the RESP calculated with α^{max} compared to the RESP without it is larger than a threshold (fixed to 0.7% here), then the candidate shell is retained and added to the current basis, and the algorithm goes back to step 1 for the same angular momentum l . If the relative deviation is lower than the threshold, then no shell is retained, and the process goes back to step 1 with an incremented l .

Figure 2 illustrates the main steps of the optimization procedure. Figure 2(a) shows the RESP deviation as a function of the additional Gaussian exponents $\{\alpha^{(i)}\}$ for d orbitals. The first iteration brings a large increase of the RESP (up to 30%) with respect to the current basis that contained no d orbitals. Once the maximizing exponent is chosen ($\alpha = 2.0$, large green circle on the curve), the second iteration shows lower deviations with respect to the current basis (with one d orbital). The second maximizing exponent ($\alpha = 4.0$, large green circle on the curve) is selected. The procedure is continued until the deviation is lower than 0.7%. After that, the orbital momentum is incremented, and the procedure is repeated until the orbital momentum is equal to $l_{\max} = 7$. Figure 2(b) shows the weighted electronic stopping power dependence on the impact parameter for the selected exponents (the details of the

geometric weighting factor can be found in the Appendix). The stopping power increases for each subsequent iteration for all of the projectile impact parameters. Adding more shells was particularly important for the low-impact parameters p around 0.2–0.4 Å, where the core electrons reside. Finally, Fig. 2(c) presents the RESP relative deviation for each iteration. Since in the starting basis set opt0 many s and p orbitals were already included, one does not see a very large change corresponding to the addition of the basis functions with these orbital momenta. The largest change occurs for the d orbital. For every orbital momentum, the convergence is quite fast (five orbitals per l are needed at most). The functions with high orbital momenta do have non-negligible contributions. We stop our optimization at $l_{\max} = 7$, however, because the last included shell for l_{\max} brought only a small increase of the RESP.

In practice, in order to obtain a basis set that can be used for the stopping power calculations for the complete projectile velocity range, we perform the optimization procedure for two projectile velocities: We start with $v = 4.0$ a.u., where the basis is very sensitive to the core electrons, as explained above. Then, we start the procedure over with this optimized basis set as a starting basis (opt0) for a low velocity $v = 0.5$ a.u. We observe that the second iteration at low velocity adds more diffuse functions that describe the valence electron excitations. After the second optimization run (at $v = 0.5$ a.u.) we obtain around 40% more basis functions. We call the final optimized basis opt-k, which stands for the optimized basis up to $l = 7$ (k is the angular momentum).

In order to compare the resulting optimized basis set with the standard one, we present the square roots of the inverse of Gaussian exponents $1/\sqrt{\alpha}$ in Fig. 3 for our optimized basis opt-k against the Dunning aug-cc-pCV6Z. These values are the length scale of a Gaussian function $e^{-\alpha r^2}$.

We observe significant differences between opt-k and aug-cc-pCV6Z: The values of $1/\sqrt{\alpha}$ of the opt-k basis are mostly concentrated in the 0.25–1.0-Å region. This region precisely

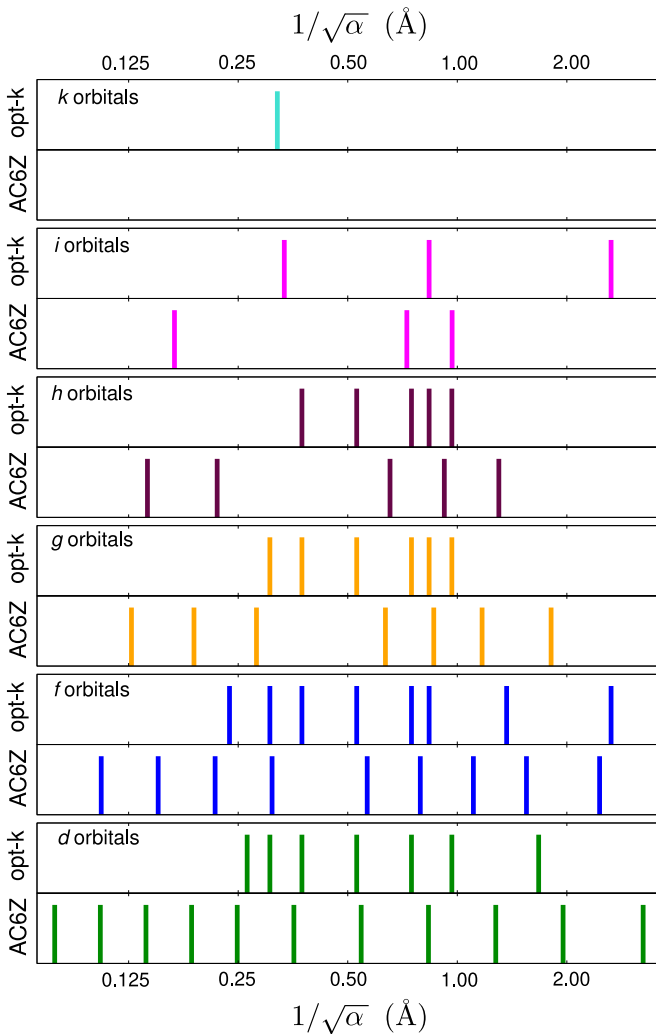


FIG. 3. Comparison of spatial extensions of the optimized basis opt-k with the most complete standard aug-cc-pCV6Z (abbreviated as AC6Z) for a proton in aluminum.

corresponds to the projectile impact parameters at which the stopping power weight has the largest values. The standard aug-cc-pCV6Z basis contains a lot of basis functions with the exponents outside the mentioned region, which do not have a significant contribution to the stopping power values. Automatically, the generated basis follows the same trend as the Dunning basis: The higher the angular momentum is, the fewer shells are needed.

Finally, we generate the basis sets for aluminum and lithium targets. We compare the RESP as a function of the proton velocity calculated with the optimized basis with the values obtained with the largest Dunning basis sets available for these elements (Fig. 4).

In the case of the aluminum target, the optimized basis provides slightly larger values than the Dunning basis, and the numerical cost is decreased. The optimized opt-k basis contains 293 basis functions per atom, whereas the Dunning basis aug-cc-pCV6Z has 324 per atom. Even though the difference in the number of basis functions is not very large, the computational time has a cubic dependence on the number

of basis functions, and therefore, the cost of calculations using opt-k is 1.5 lower than that for the aug-cc-pCV6Z basis.

For the lithium cluster, the situation is different: The largest available Dunning basis is only cc-pCQZ ($l_{\max} = 4$, and the diffuse functions are not included). Hence, with the optimized basis opt-k ($l_{\max} = 7$), one obtains remarkably more converged stopping power values. The agreement with respect to the experiment is much improved, as shown in Fig. 4(b).

The basis set optimization procedure has allowed us to obtain more converged electronic stopping power. This becomes crucial when the available standard basis sets are limited to low angular momenta as in the case of Li. In addition, by tuning the tolerance of the algorithm (the deviation threshold that was chosen to be 0.7% in this work), one can choose the precision of the basis. This generation scheme is hence flexible in terms of the number of basis functions, while the standard basis sets provide rather a discrete choice of basis with an integral cardinal number X .

IV. RESULTS

A. Comparison with experiments and other calculations

We compare our most converged results using our basis set opt-k to other *ab initio* and experimental results for the proton and α -particle irradiation in the aluminum target in Fig. 5. In addition to our results, we plot the RT-TDDFT calculations obtained with the plane-wave code QBOX [17] and with linear-response TDDFT (LR-TDDFT) calculations with the plane-wave code ABINIT [28]. The experimental values are taken from the SRIM reference [38]. The experimental values are interpolated with the empirical codes PSTAR (for the proton), ASTAR (for the α particle) [39], and SRIM (for both projectiles) [38].

For the proton irradiation in aluminum [Fig. 5(a)], in the low-velocity regime, all three *ab initio* results are in good agreement with the experimental data and with the empirical codes (SRIM and PSTAR). Our localized basis calculations yield slightly larger values, however. Then, around the peak, all the *ab initio* codes provide larger values than SRIM and PSTAR. It is difficult to comment on the agreement with the experiment since the discrepancy among experimental data is large in this region (around 35%). However, for larger proton velocities ($v \geq 4.0$ a.u.), the experimental points follow more or less the same line, and it is clearly seen that all of the presented *ab initio* results are lower than the experimental data and the empirical codes.

For the α -particle projectile in aluminum [Fig. 5(b)], we use the basis set optimized for a proton in aluminum. We assume the basis set generated especially for the α particle is similar to the one generated for the proton. The investigation of the influence of the projectile on the optimized basis sets is left for future work.

For this system, one can note a similar trend among the two independent RT-TDDFT results in comparison with the experiment: underestimation of the RT-TDDFT stopping power with respect to SRIM and ASTAR at high projectile velocities. For the linear response result, the random stopping power of the α particle is simply $4 \times S^{\text{H}^+}$, where S^{H^+} is the random stopping power of a proton. For the α -particle velocities

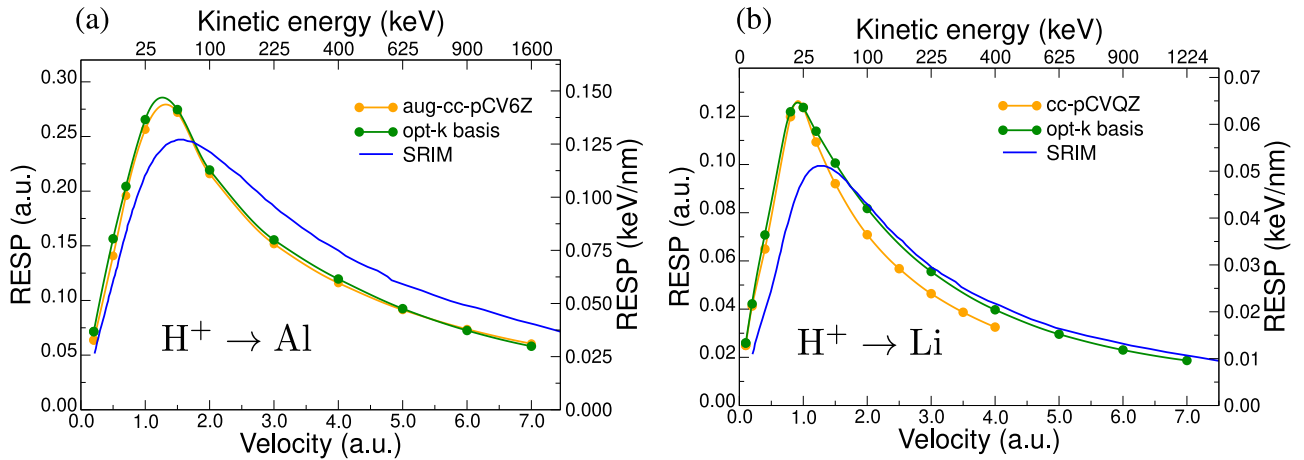


FIG. 4. Random electronic stopping power of a proton in (a) aluminum and (b) lithium targets. The calculations were performed using the largest available Dunning basis sets for each target (orange curves) and the basis sets created in this work (opt-k, green curves). The results are compared to the empirical code SRIM values [38] (blue curves).

$v > 3.0$ a.u., the linear response results are in very good agreement with the two RT-TDDFT results. However, LR-TDDFT overestimates greatly the RT-TDDFT and experimental values for the projectile velocities around the stopping power peak and below. Indeed, the linear response theory does not account for the charge reorganization around the projectile, and this becomes critical for slow and multiply charged projectiles.

We would like to focus here on the large-velocity regime, for which all the *ab initio* results are in agreement and underestimate the empirical codes and the experimental points. In addition, such behavior is common to most comparisons between *ab initio* and experimental results for different materials: for example, silicon carbide [40], liquid water [29], silicon [23], and nickel [24].

First, a possible source of discrepancy among the *ab initio* results is the inclusion or not of the Al $1s$ electrons. In the work of Schleife and coworkers [17] as well as in the work

of Shukri and coworkers [28], pseudopotentials that treat $2s2p3s3p$ electrons explicitly were used. This implies that the $1s$ electron excitations were not taken into account in these calculations. Therefore, the difference between those results and the experimental points could come from the neglect of the $1s$ excitations.

To evaluate the contribution of $1s$ electrons to the stopping power in aluminum, we performed the RT-TDDFT simulations with manually frozen $1s$ electrons. The details of the freezing procedure are given in Ref. [31]. The results reported in Fig. 6(a) show that there is almost no influence of the Al $1s$ electrons. The largest difference ($\sim 0.2\%$) is obtained for the largest projectile velocity used in our calculations. The absence of the $1s$ excitations can be explained by their very low energies: around 1500 eV below the Fermi level.

Second, the role of the approximate exchange-correlation functional in the high-velocity underestimation needs to be

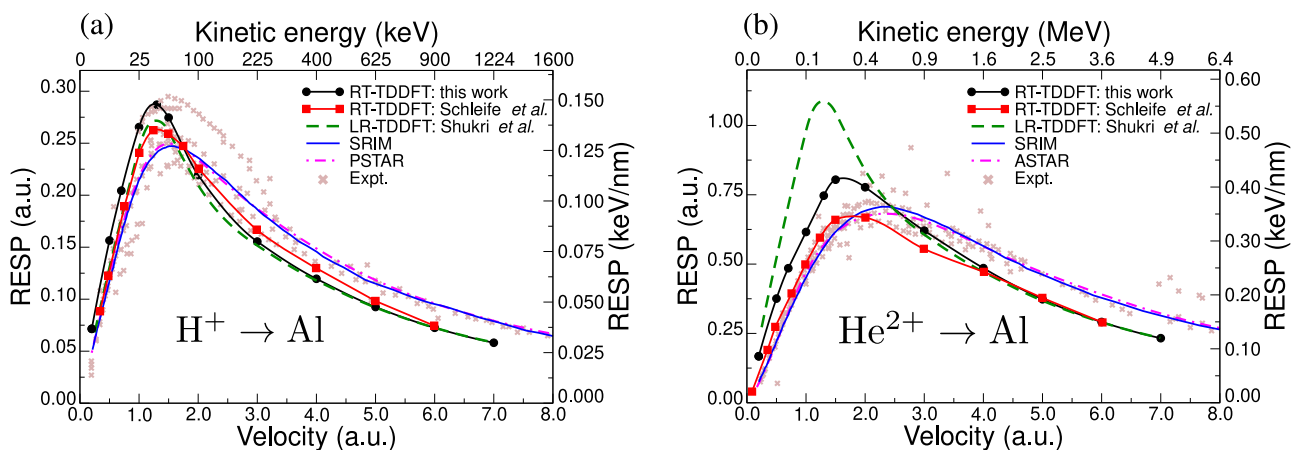


FIG. 5. Random electronic stopping power of (a) a proton and (b) α particle in aluminum as a function of the projectile velocity. RT-TDDFT results obtained in this work are in black. The RT-TDDFT plane-wave code results from Ref. [17] are presented in red. The LR-TDDFT plane-wave curves (dashed green lines) come from Ref. [28]. All the *ab initio* results are obtained with the LDA exchange-correlation functional. Experimental points are taken from the SRIM online database [38]. SRIM and PSTAR/ASTAR [39] interpolation curves are depicted in blue and pink, respectively.

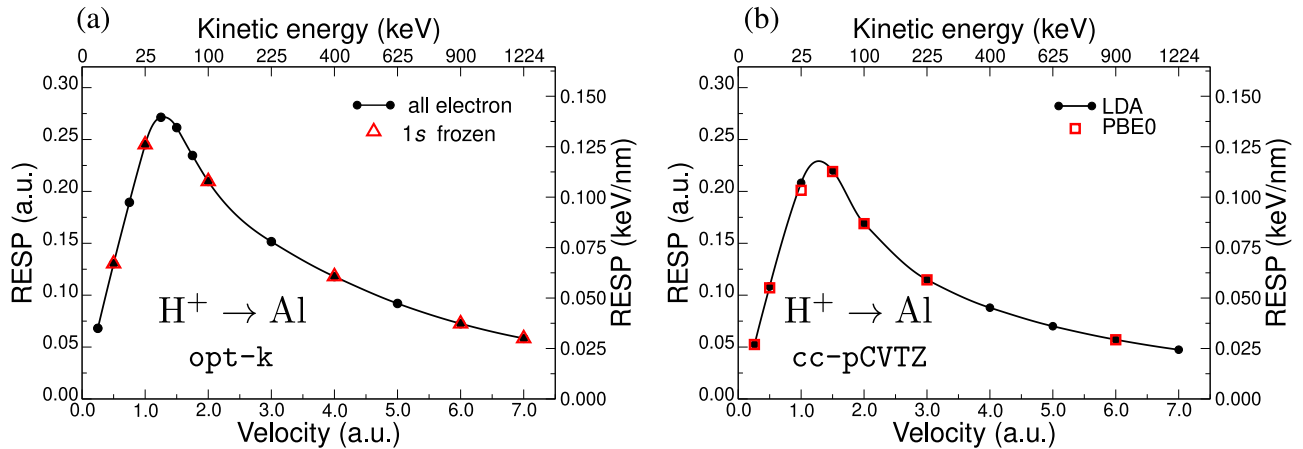


FIG. 6. Random electronic stopping power of a proton in aluminum. (a) Comparison between the all-electron dynamics and the dynamics with $1s$ frozen electrons (in the opt-k basis set). (b) Comparison between LDA and PBE0 exchange-correlation functionals (in the cc-pCVTZ basis set).

analyzed as a possible cause of the error. Very few TDDFT calculations for ion irradiation use exchange-correlation functionals beyond the semilocal approximations [23,29].

With our localized orbital implementation, it is possible to use hybrid functionals at a reasonable cost. Hybrid functionals include a fixed amount of exact exchange [41]. Here we test the effect of the celebrated PBE0 approximation [42] that incorporates 25% of exact-exchange. Figure 6(b) compares the PBE0 result to the local-density approximation (LDA) result. These calculations were performed in a smaller cc-pCVTZ basis set because of the large computational cost. The change in exchange-correlation functional leads to only a minor difference in the RESP: The largest change occurs for $v = 1.0$ a.u. and is as low as 4%. The negligible effect of the exchange-correlation functional is confirmed for several other functionals in metallic lithium (not shown here).

Hence, the reason for the systematic underestimation of all the *ab initio* calculations at high projectile velocities is still unclear and requires further investigation.

B. Core state contribution: Impact parameter dependence

Even though it is a known fact that the core electrons play an important role in the stopping power calculations [17,23,28], we would like to quantify the contributions of the core electron levels as a function of the projectile velocity.

To do this, we use a technique similar to what was applied above for $1s$ levels: We calculate the RESP with a varying range of frozen states, $S_e^{1s \text{ frozen}}$, $S_e^{1s 2s \text{ frozen}}$, and $S_e^{1s 2s 2p \text{ frozen}}$. Even though the definition of each contribution is not unique (the stopping power is not a simple sum of the terms arising from the different electronic levels), the linearity almost holds in practice. We define the valence electron-only contribution as $S_e^{\text{val}} = S_e^{1s 2s 2p \text{ frozen}}$. Then, the contribution of the $1s$ electrons is taken to be $S_e^{1s} = S_e^{\text{total}} - S_e^{1s \text{ frozen}}$. In a similar way, we determine the contributions of $2s$ electrons as $S_e^{2s} = S_e^{1s \text{ frozen}} - S_e^{1s 2s \text{ frozen}}$ and $2p$ electrons as $S_e^{2p} = S_e^{1s 2s \text{ frozen}} - S_e^{1s 2s 2p \text{ frozen}}$. Note that with this core-freezing technique, the full nodal structure of the valence wave functions is conserved, in contrast to the pseudopotential approach.

Figure 7(a) presents the electron contributions to the RESP as a function of the projectile velocity. It is seen that at the stopping power peak ($v = 1.0$ a.u.) the contribution of the core electrons ($2s 2p$) is still very limited (lower than 1%). However, for $v \geq 4.0$ a.u. the core electron contribution is 50% or larger. The contribution of the $2p$ electrons appears at a lower velocity than the $2s$ electrons because the binding energy of these electrons is noticeably weaker (65 versus 102 eV). These numbers show the necessity of including the core electron excitations for the medium to large projectile velocities.

Figure 7(b) shows the impact parameter dependence of the stopping power divided into different electronic level contributions. We have selected the proton velocity $v = 4$ a.u. for this analysis. As expected, the contributions of the core electrons ($2s$ and $2p$) are larger for impact parameters close to the nuclei. Remarkably, the contribution of valence electrons is very flat. Note that despite the visible predominance of the $2s$ and $2p$ curves, for the RESP calculation, multiplication by the geometric weighting function (see the Appendix) will reduce these contributions.

C. Centroid path approximation validity

Now we would like to discuss the accuracy of the so-called centroid path approximation in the RESP calculations. This approximation was introduced in Ref. [43] and is regularly used in more recent RESP evaluation [23,29]. The centroid path approximation states that the *random* electronic stopping power can be safely evaluated with a single trajectory located at the geometric center of the unit tile (the centroid). In other words, the approximation states that the impact-parameter-averaged stopping power is the stopping power at the averaged impact parameter.

Our sampling scheme recalled in the Appendix assumes only the polar symmetry of the impact-parameter-dependent stopping power. The error induced by this mild approximation has been quantified to be lower than 2% [25]. Our approach can serve as a reference to evaluate the performance of the centroid approximation.

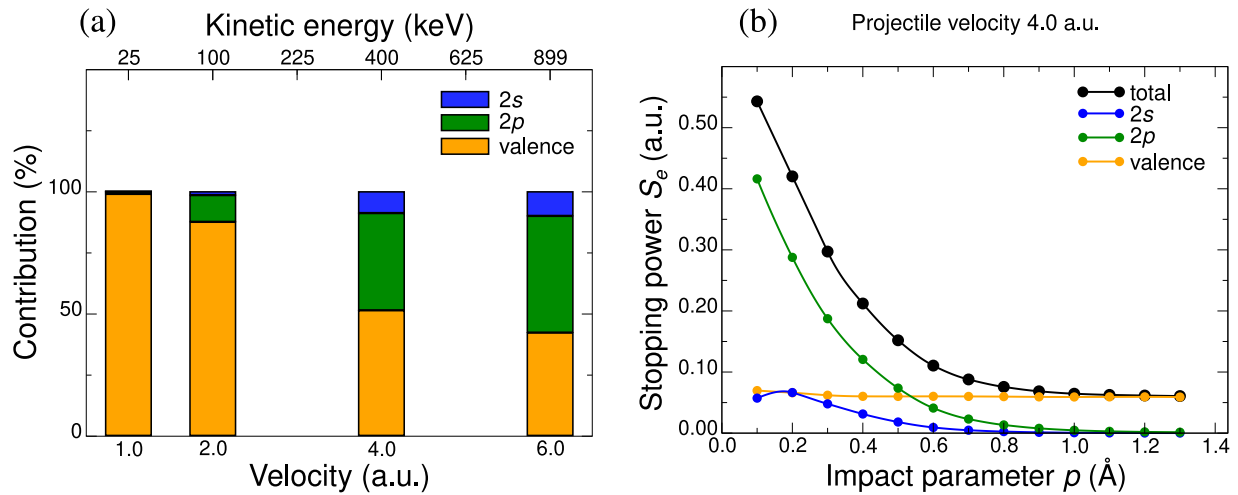


FIG. 7. (a) Relative contributions to the random electronic stopping power of 2s (blue), 2p (green), and valence (orange) electrons as a function of the projectile velocity for a proton in aluminum. (b) Same contributions as a function of the proton impact parameter p for fixed proton velocity $v = 4.0$ a.u. Being negligible, the 1s contribution is not presented.

The centroid approximation was validated in calculations for which the core electrons were not needed or kept frozen [23,29,43]. In Fig. 8, we reproduce such a statement: We compare the centroid approximation to the complete averaging for a proton in aluminum, where the core electrons ($1s2s2p$) have been kept frozen. The two dashed lines coincide very convincingly, which validates the centroid approximation in this case. However, when comparing the total stopping powers without freezing the core electrons, the two solid lines depart very much from each other. For large velocities, the centroid approximation leads to errors up to 35% in RESP.

The observations can be understood by keeping in mind the weak impact parameter dependence of the valence electrons, as shown in Fig. 7(b). The core electrons do have a strong impact parameter dependence.

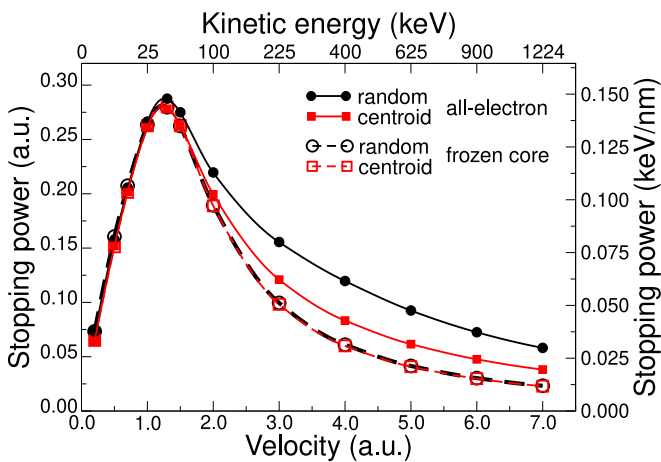


FIG. 8. Random electronic stopping power calculated within the impact parameter averaging (black curves) and the centroid path approximation (red curves) for a proton in aluminum. Solid lines correspond to the all-electron dynamics; dashed lines correspond to the frozen-core simulations.

Finally, we conclude that the centroid approximation should be employed with great care: As soon as core electrons are involved, e.g., for large velocities, it is not justified anymore. Our findings are further confirmed by calculations for metallic lithium (not shown here), where the core electrons are much less bound.

V. CONCLUSIONS

In this work, we have demonstrated that the RT-TDDFT *ab initio* simulations performed within the localized Gaussian basis sets can provide accurate electronic stopping power results provided that sufficiently large basis sets are used. The standard basis sets that were developed to describe the correlation energy are not well adapted for the stopping power calculations. Therefore, we have proposed a simple basis set generation approach based on the observation that more accurate basis sets correspond to a higher electronic stopping power.

Following this automated procedure, we have developed here stopping-power-oriented basis sets for lithium and aluminum. The lithium basis has allowed us to produce RESP for proton irradiations in metallic lithium with unprecedented accuracy. The aluminum basis has permitted us to compare very well with earlier independent plane-wave calculations [17] for proton and α -particle irradiations. We confirm a serious underestimation of the TDDFT results in aluminum for high velocities.

The localized orbital framework has a moderate computational cost (about 1300 core hours on Intel Skylake processors per velocity per impact parameter). It further allows one to conduct specific calculations that would be very difficult in plane waves, such as the inclusion of the deep-core electrons and the use of hybrid functionals of DFT.

We have concluded that the 1s electrons of aluminum do not participate in the stopping process at the considered velocities. Also, we have verified that the hybrid exchange-correlation functionals do not lead to significant changes in the

stopping power in aluminum. Using a frozen-core technique, we have analyzed the contribution of the core levels to the stopping power as a function of the projectile velocity.

Finally, based on the proton in aluminum example, we have shown the importance of accurate impact parameter sampling for the RESP calculations. In particular, the handy, but dangerous, centroid path approximation should be limited to those cases where core electrons do not contribute to RESP.

ACKNOWLEDGMENT

This work was performed using HPC resources from GENCI-CINES and GENCI-TGCC (Grant No. 2020-096018).

APPENDIX: RANDOM ELECTRONIC STOPPING POWER SAMPLING

For the sake of completeness, we recall our numerical scheme for the random electronic stopping power (RESP) calculations presented in Ref. [25]. We use the ensemble average technique: The RESP values $\langle S_e(v) \rangle$ (at a given target orientation) are obtained as the average of the stopping power over the projectile impact parameter \mathbf{p} :

$$\langle S_e(v) \rangle = \frac{1}{\mathcal{A}} \int d\mathbf{p} S_e(v, \mathbf{p}), \quad (\text{A1})$$

where \mathcal{A} is the area of the tile that completely paves the surface perpendicular to the projectile beam and $S_e(v, \mathbf{p})$ is the electronic stopping power for a projectile trajectory corresponding to an impact parameter \mathbf{p} . We have found that in Li and Al the electronic stopping power is sensitive to only the absolute value of the impact parameter p . Due to this fact, we transform the two-dimensional integration over the vector

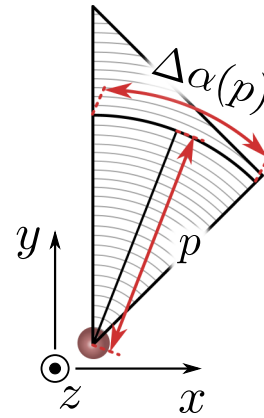


FIG. 9. Illustration of the stopping power integration. A case of the fcc [001] crystal plane. The elementary tile for the impact parameter integration is the triangle. One assumes that the stopping power depends only on the module of the impact parameter p . Then, for the integration, one needs to take into account the length of the arc $p\Delta\alpha(p)$ as a function of p . The target atom is depicted as a pink sphere.

\mathbf{p} to one-dimensional integration over the absolute value p :

$$\langle S_e(v) \rangle = \frac{1}{\mathcal{A}} \int_0^{p_{\max}} dp p \Delta\alpha(p) S_e(v, p), \quad (\text{A2})$$

where $\Delta\alpha(p)$ is the angular range of the arc contained in the elementary tile at each distance p (Fig. 9), $p = 0$ corresponds to the head-on collision, and p_{\max} is the maximal impact parameter within the tile \mathcal{A} along a selected axis. In this way, $p\Delta\alpha(p)$ is the weight assigned to the stopping power $S_e(v, p)$ when averaging over the crystalline plane. The factor $p\Delta\alpha(p)$ can also be interpreted as the probability to impinge the crystal at the impact parameter p .

-
- [1] S. Pellegrino, P. Trocellier, S. Miro, Y. Serruys, É. Bordas, H. Martin, N. Chaâbane, S. Vaubaillon, J. Gallien, and L. Beck, *Nucl. Instrum. Methods Phys. Res. Sect. B* **273**, 213 (2012).
- [2] R. Mohan and D. Grosshans, *Adv. Drug Deliv. Rev.* **109**, 26 (2017).
- [3] H. Kraus, D. Simin, C. Kasper, Y. Suda, S. Kawabata, W. Kada, T. Honda, Y. Hijikata, T. Ohshima, V. Dyakonov *et al.*, *Nano Lett.* **17**, 2865 (2017).
- [4] Y. Katoh, N. Hashimoto, S. Kondo, L. Snead, and A. Kohyama, *J. Nucl. Mater.* **351**, 228 (2006).
- [5] G. Was, *Fundamentals of Radiation Materials Science* (Springer, New York, 2017), pp. 45–60.
- [6] J. Lindhard and M. Scharff, *Mat. Fys. Medd. K. Dan. Vidensk. Selsk.* **27**, 1 (1953).
- [7] G. J. Iafrate and J. F. Ziegler, *J. Appl. Phys.* **50**, 5579 (1979).
- [8] P. Echenique, R. Nieminen, and R. Ritchie, *Solid State Commun.* **37**, 779 (1981).
- [9] I. Nagy, A. Arnau, and P. M. Echenique, *Phys. Rev. A* **40**, 987 (1989).
- [10] A. Arnau, M. Penalba, P. M. Echenique, F. Flores, and R. H. Ritchie, *Phys. Rev. Lett.* **65**, 1024 (1990).
- [11] S. T. Manson, *Phys. Rev. A* **6**, 1013 (1972).
- [12] L. L. Balashova, N. M. Kabachnik, and V. N. Kondratyev, *Phys. Status Solidi B* **161**, 113 (1990).
- [13] E. H. Mortensen, J. Oddershede, and J. R. Sabin, *Nucl. Instrum. Methods Phys. Res. Sect. B* **69**, 24 (1992).
- [14] E. Runge and E. K. U. Gross, *Phys. Rev. Lett.* **52**, 997 (1984).
- [15] A. A. Correa, *Comput. Mater. Sci.* **150**, 291 (2018).
- [16] F. Gygi, *IBM J. Res. Dev.* **52**, 137 (2008).
- [17] A. Schleife, Y. Kanai, and A. A. Correa, *Phys. Rev. B* **91**, 014306 (2015).
- [18] A. Castro, H. Appel, M. Oliveira, C. A. Rozzi, X. Andrade, F. Lorenzen, M. A. Marques, E. Gross, and A. Rubio, *Phys. Status Solidi B* **243**, 2465 (2006).
- [19] J. M. Soler, E. Artacho, J. D. Gale, A. García, J. Junquera, P. Ordejón, and D. Sánchez-Portal, *J. Phys.: Condens. Matter* **14**, 2745 (2002).
- [20] J. M. Pruneda, D. Sánchez-Portal, A. Arnau, J. I. Juaristi, and E. Artacho, *Phys. Rev. Lett.* **99**, 235501 (2007).
- [21] J. Hutter, M. Iannuzzi, F. Schiffmann, and J. VandeVondele, *Wiley Interdiscip. Rev.: Comput. Mol. Sci.* **4**, 15 (2014).
- [22] F. Bruneval, T. Rangel, S. M. Hamed, M. Shao, C. Yang, and J. B. Neaton, *Comput. Phys. Commun.* **208**, 149 (2016).
- [23] D. C. Yost, Y. Yao, and Y. Kanai, *Phys. Rev. B* **96**, 115134 (2017).

- [24] R. Ullah, E. Artacho, and A. A. Correa, *Phys. Rev. Lett.* **121**, 116401 (2018).
- [25] I. Maliyov, J.-P. Crocombette, and F. Bruneval, *Eur. Phys. J. B* **91**, 172 (2018).
- [26] J. Nobel, S. Trickey, J. R. Sabin, and J. Oddershede, *Chem. Phys.* **309**, 89 (2005).
- [27] A. Szabó and N. S. Ostlund, *Modern Quantum Chemistry: Introduction to Advanced Electronic Structure Theory* (Dover Publications, Mineola (NY), 1996).
- [28] A. A. Shukri, F. Bruneval, and L. Reining, *Phys. Rev. B* **93**, 035128 (2016).
- [29] D. C. Yost and Y. Kanai, *Phys. Rev. B* **94**, 115107 (2016).
- [30] D. C. Yost and Y. Kanai, *J. Am. Chem. Soc.* **141**, 5241 (2019).
- [31] I. Maliyov, Ph.D. thesis, Université Paris Saclay, 2019.
- [32] T. H. Dunning, Jr., *J. Chem. Phys.* **90**, 1007 (1989).
- [33] R. A. Kendall, T. H. Dunning, Jr., and R. J. Harrison, *J. Chem. Phys.* **96**, 6796 (1992).
- [34] D. E. Woon and T. H. Dunning, Jr., *J. Chem. Phys.* **98**, 1358 (1993).
- [35] Y. Yao, D. C. Yost, and Y. Kanai, *Phys. Rev. Lett.* **123**, 066401 (2019).
- [36] S. Lehtola, *J. Comput. Chem.* **36**, 335 (2015).
- [37] E. Coccia and E. Luppi, *Theor. Chem. Acc.* **135**, 43 (2016).
- [38] J. F. Ziegler, M. D. Ziegler, and J. P. Biersack, *Nucl. Instrum. Methods Phys. Res. Sect. B* **268**, 1818 (2010).
- [39] M. J. Berger, M. Inokuti, H. H. Andersen, H. Bichsel, D. Powers, S. M. Seltzer, D. Thwaites, and D. E. Watt, *J. ICRU* **os25**, 76 (1993).
- [40] K. G. Reeves, Y. Yao, and Y. Kanai, *Phys. Rev. B* **94**, 041108(R) (2016).
- [41] J. P. Perdew, *MRS Bull.* **38**, 743 (2013).
- [42] C. Adamo and V. Barone, *J. Chem. Phys.* **110**, 6158 (1999).
- [43] A. Ojanperä, A. V. Krasheninnikov, and M. Puska, *Phys. Rev. B* **89**, 035120 (2014).